Title

Free-breathing variable flip angle balanced SSFP cardiac cine imaging with reduced SAR at 3T

Journal

Magnetic Resonance in Medicine, 76(4)

ISSN

0740-3194

Authors

Srinivasan, Subashini
Kroeker, Randall M
Gabriel, Simon
et al.

Publication Date

2016-10-01

DOI

10.1002/mrm.26011

Peer reviewed

NOTE

Magnetic Resonance in Medicine 00:00–00 (2015)

Free-Breathing Variable Flip Angle Balanced SSFP Cardiac Cine Imaging with Reduced SAR at 3T

Subashini Srinivasan,[1,2] Randall M. Kroeker,[3] Simon Gabriel,[1] Adam Plotnik,[1] Sergio R. Godinez,[1] Peng Hu,[1,4] Nancy Halnon,[5] J. Paul Finn,[1,4] and Daniel B. Ennis[1,2,4]*

Purpose: To develop a free-breathing variable flip angle (VFA) balanced steady-state free precession (bSSFP) cardiac cine imaging technique with reduced specific absorption rate (SAR) at 3 Tesla.

Methods: Free-breathing VFA (FB-VFA) images in the short-axis and four-chamber views were acquired using an optimal VFA scheme, then compared with conventional breath-hold constant flip angle (BH-CFA) acquisitions. Two cardiac MRI experts used a 5-point scale to score images from healthy subjects (N = 10). The left ventricular ejection fraction, end diastolic volume (LVEDV), end systolic volume, stroke volume (LVSV), and end diastolic myocardial mass (LVEDM) were determined by manual contour analysis for BH-CFA and FB-VFA. A pilot evaluation of FB-VFA was performed in one patient with Duchenne muscular dystrophy.

Results: FB-VFA SAR was 25% lower than BH-CFA with similar blood–myocardium contrast. The qualitative FB-VFA score was lower than the BH-CFA for the short-axis (3.1 ± 0.5 versus 4.3 ± 0.8; $P < 0.05$) and the four-chamber view (3.4 ± 0.4 versus 4.6 ± 0.6; $P < 0.05$). The LVEDV and the LVSV were 5% and 12% larger ($P < 0.05$) for FB-VFA compared with BH-CFA. There was no difference in LVEDM.

Conclusion: FB-VFA bSSFP cardiac cine imaging decreased the SAR at 3T with image quality sufficient to perform cardiac functional analysis. **Magn Reson Med 000:000–000, 2015.**

Key words: free-breathing cardiac cine imaging; variable flip angle; bSSFP

INTRODUCTION

The evaluation of cardiac function with MRI for pediatric patients with known or suspected heart disease is central to their clinical evaluation, but poses several challenges, especially at 3 Tesla (T). In general, very young pediatric patients frequently exhibit low or moderate compliance with breath-holding instructions, leading to image artifacts or repeated scans. More specifically, pediatric patients with Duchenne muscular dystrophy (DMD) have an inherited muscular disorder that affects all striated muscle resulting in skeletal muscle, respiratory muscle, and cardiac muscle function impairment (1,2) and may significantly limit breath-hold capacity especially for older pediatric patients. Therefore, alleviating the need for breath-holding while maintaining diagnostic image quality remains an unmet clinical need.

Free-breathing cardiac cine imaging can be performed to reduce image artifacts due to poor breath-holding and simultaneously improve patient comfort. Respiratory motion compensation can be performed using navigator echoes (3), but the application of the navigator echoes limits capturing the entire cardiac cycle and can disrupt the steady-state signal leading to image artifacts. Herein we have adopted the approach of Kellman et al (4) and acquired the images continuously in real time, then retrospectively binned and reconstructed conventional cine images.

In addition to the challenge of a multiple breath-hold cardiac MRI exam in patients with poor respiratory function, pediatric patients appear to have a heightened sensitivity to heating, hence there exists a need to consider methods that can reduce radiofrequency (RF) induced heating. Cardiac cine imaging is particularly well suited for evaluating cardiac function with balanced steady-state free precession (bSSFP) due to its high signal-to-noise ratio (SNR) efficiency and high blood–myocardium contrast (5,6). However, bSSFP imaging at 3T can have notably increased SAR compared with 1.5T, due to the use of high imaging flip angles that produce high blood–myocardium contrast (7,8). Furthermore, because free-breathing acquisitions have extended RF deposition intervals compared with breath-hold acquisitions, the RF induced heating will be sustained for a longer duration and may lead to increased patient discomfort.

We sought to overcome these two challenges of conventional breath held constant flip angle (BH-CFA) bSSFP by developing and evaluating a free-breathing (FB) cardiac cine bSSFP imaging exam at 3T that: (i) reduces the specific absorption rate (SAR) by using an optimized variable flip angle scheme (FB-VFA) (9,10); and (ii) compensates for respiratory motion using real-time acquired cardiac images that are retrospectively binned using bellows gating (11,12) to alleviate the need for breath-holding.

[1]Department of Radiological Sciences, University of California, Los Angeles, California, USA.

[2]Department of Bioengineering, University of California, Los Angeles, California, USA.

[3]Siemens Canada Limited, Winnipeg, Manitoba, Canada.

[4]Biomedical Physics Interdepartmental Program, University of California, Los Angeles, California, USA.

[5]Department of Pediatrics, University of California, Los Angeles, California, USA.

Grant sponsor: UCLA's Center for Duchenne Muscular Dystrophy; Grant sponsor: American Heart Association; Grant sponsor: Siemens Medical Solutions.

*Correspondence to: Daniel B. Ennis, Ph.D., Peter V. Ueberroth Building, Suite 1471, Room B, 10945 Le Conte Avenue, Los Angeles, CA 90095.
E-mail: daniel.ennis@ucla.edu

Received 9 April 2015; revised 15 September 2015; accepted 15 September 2015

DOI 10.1002/mrm.26011

Published online 00 Month 2015 in Wiley Online Library (wileyonlinelibrary.com).

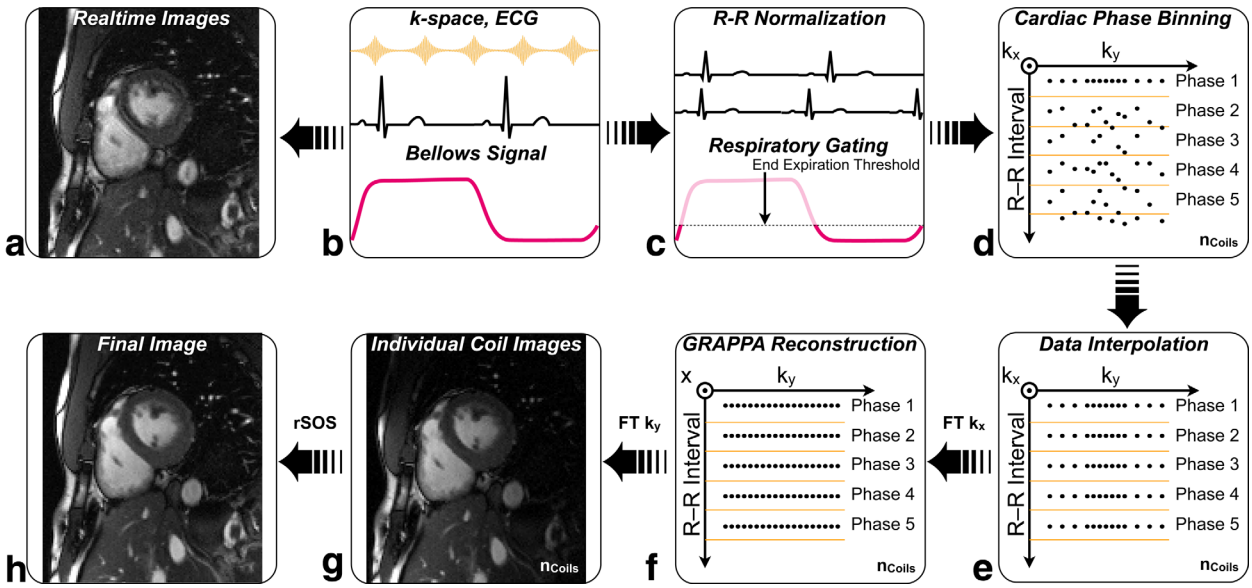

FIG. 1. Cardiac cine reconstruction scheme for the free-breathing, bellows gated, variable flip angle (FB-VFA) technique. **B:** The ECG and the bellows signal were recorded during the acquisition of each k_y-line. **A:** The acquired k-space data were Fourier transformed (FT) to real-time cardiac images. **C:** The R-R interval was normalized to account for R-R interval variation and k_y lines outside the respiratory gating window were discarded. Each k_y line was sorted based on the ECG timestamp (**D**) and linearly interpolated into the number of desired cardiac phases (**E**). **F:** The data were FT along the k_x direction and GRAPPA reconstruction was used to fill the missing k_y lines. The individual coil data (**G**) were combined for each cardiac phase to form the final cardiac cine images (**H**).

METHODS

Choice of Optimal Variable Flip Angle Scheme

A previously reported VFA bSSFP approach for cardiac cine imaging was adapted herein to lower the SAR of the acquisition without significantly altering the blood–myocardium contrast or point spread function (PSF) (9) compared with the conventional CFA k-space segmented acquisition. The Bloch simulations for different VFA schemes with imperfect slice profile and flowing blood (7,13) were performed in MATLAB (The Mathworks, Natick, MA) identical to Srinivasan and Ennis (9) with the following modified parameters for 3T imaging: T_1/T_2 of stationary myocardium = 1471/47 ms, $T_1/T_2/T_2^*$ of flowing blood = 1932/275/138 ms (14), repetition time (TR) = 2.8 ms, echo time (TE) = 1.4 ms, 93 RF pulses per measurement (N_{ky}), and 10 consecutive measurements.

The signal simulations were repeated for every combination of N_{ramp} between 20 to 45 in steps of five pulses, N_{low} between zero to 25 in steps of five pulses, $\alpha_{low} = 5^\circ$ to 40° in steps of 5° and $\alpha_{high} = [40^\circ, 50^\circ]$. The minimum α_{high} was chosen to be 40° as the CFA cardiac cine acquisition was SAR limited for higher FAs at 3T. The choice of lower limit of $N_{ramp} = 20$ was chosen (9) to reduce signal oscillations during the transition between steady states. As not all combinations are realizable, any combination of VFA scheme with negative $N_{high} = N_{ky} - (2 \times N_{ramp} + 2 \times N_{low})$ was not simulated. The blood–myocardium contrast and full width half max (FWHM) of the PSF for each VFA scheme and CFA = 40° were calculated from the last measurement (9). The relative deposited RF energy with respect to CFA = 40° was estimated for each of these VFA schemes as the ratio of sum of squares of individual flip angles of the VFA scheme to the sum of squares of CFA of 40°.

The final optimal VFA scheme was chosen by selecting a sub-set of these VFA schemes with contrast $\geq$ CFA = 40°, with relative deposited RF energy < 1 and relative FWHM of PSF ≤ 1.2. Among these, the VFA scheme with the least SAR was chosen as the optimal VFA scheme.

Bellows Gated VFA Imaging Acquisition and Reconstruction

The different steps used in the reconstruction of FB-VFA cardiac cine images are illustrated in Figure 1. Respiratory motion compensation for FB-VFA was performed using bellows gating. The VFA cardiac images were continuously acquired to maintain the dynamic steady-state signal. The bellows signal and the electrocardiogram (ECG) timestamp from the QRS trigger were recorded during the acquisition of each k_y line. The R-R interval variations were adjusted by normalizing the ECG timestamps of data within any given R-R interval to the actual R-R duration. The respiratory gating window was chosen by setting a patient specific threshold on the bellows signal (25% to 35%). The k-space lines within the respiratory gating window were sorted based on their normalized ECG timestamp and linearly interpolated in time into the desired number of cardiac phases individually for each coil. This ECG timestamp and bellows gating-based rebinning of k-space were implemented on the Siemens scanner, and the data were further reconstructed using the manufacturer's reconstruction pipeline, which included GRAPPA (15).

In Vivo Imaging Experiments

BH-CFA and FB-VFA cardiac exams were performed in 10 healthy subjects (N = 10, 9 male, age = 29 $\pm$ 5 years) subsequent to obtaining informed written consent using an IRB approved protocol. A pilot evaluation of the FB-VFA

technique was performed in a 26-year-old DMD patient. A mid-ventricular short-axis FB-VFA cardiac cine was acquired, after the routine BH-CFA multislice short-axis cardiac cine acquisitions.

All images were acquired on a 3T scanner (Trio, Siemens Medical Solutions, Erlangen, Germany) using a six-channel anterior cardiac coil and six-channel posterior spine matrix. Conventional two-dimensional (2D) multislice, retrospectively cardiac gated, BH-CFA bSSFP images were acquired covering the left ventricle (LV) from the apex to the base. A single four-chamber, long-axis bSSFP was also acquired using BH-CFA. Patient specific frequency scouts (16) were performed for different slices to choose the imaging frequency with the least artifacts within the LV. Each slice was acquired at the isocenter with patient-specific local cardiac shimming to reduce B_0 inhomogeneities.

The BH-CFA imaging parameters were: field of view = 360 × 303 mm, slice thickness= 6 mm, slice gap = 4 mm, 10 to 12 slices, resolution = 1.9 × 1.9 mm, TR/TE = 2.8/1.4 ms, bandwidth = 1371 Hz/px, using the maximum SAR-limited flip angle = 38.5° ± 2.4°, k_y lines per segment = 12, reconstructed cardiac phases = 20, with GRAPPA factor of two and 24 reference lines. The acquisition duration was 8 ± 1 s per slice. In addition, multislice short-axis and long-axis FB-VFA cardiac images, with VFA scheme optimized for low SAR imaging (see the Results section), were acquired with acquisition parameters matched to BH-CFA. The acquisition duration of individual VFA images was 263 ms and images were acquired continuously for 1 min.

Qualitative Image Analysis

The image quality of the mid-ventricular short-axis and long-axis slices of the BH-CFA and FB-VFA acquisitions were scored independently by two radiological experts blinded to the aim of the study and the differences between the image acquisition methods. Cines for a single mid-ventricular short-axis slice and a single long-axis slice for all subjects were displayed blinded to the acquisition scheme in a randomized manner and were scored using a 5-point scale with increments of 0.5 similar to Kellman et al (4) and Hansen et al (17) with 5 being excellent. A score of 5 indicated that the reconstruction had good blood–myocardium contrast with fine structural details readily apparent, did not have artifacts, and regional and global cardiac function was easily assessable. A score of 4 indicated that there was acceptable blood–myocardium contrast and insignificant artifacts with adequate image quality to determine global and regional cardiac function. A score of 3 was given to images with fair image quality that could be used to evaluate global and regional cardiac function, but image contrast and/or image artifacts were notable. A score of 2 was given to images where blood–myocardium contrast was poor, artifacts were significant, and/or regional function could not be determined. A score of 1 indicated non-diagnostic image quality for evaluating even global cardiac function. Half-point increments were given to images that shared criteria between integer scores. Statistical differences between the two techniques and between the observers were evaluated using Wilcoxon signed rank test with $P < 0.05$. The qualitative analysis was performed using Osirix (http://www.osirix-viewer.com/).

Quantitative Image Analysis

The LV ejection fraction (LVEF), end diastolic volume (LVEDV), end systolic volume (LVESV), stroke volume (LVSV), and end diastolic myocardial mass (LVEDM) were determined by manual contour analysis using commercial software (Argus, Siemens, Medical Systems, Erlangan, Germany) for both BH-CFA and FB-VFA acquisitions. The LV contouring of each subject's BH-CFA and FB-VFA exam were performed by experienced MRI technologists with over 10 years of experience in contouring clinical cases. Statistical differences between the two techniques were evaluated using paired, Student t-test. The t-test values were Holm-Sidak posthoc corrected.

The apparent SNR was measured in the LV blood, RV blood, and myocardial septum in both end diastolic and end systolic cardiac phases in the mid-ventricular short-axis slice using region-of-interest (ROI) analysis. The standard deviation of the noise was determined from an ROI drawn in the background region. The apparent SNR was divided by a correction factor (18) of $\sqrt{\frac{2}{4-\pi}} = 1.53$, to account for the Rayleigh distribution of the noise. Contrast-to-noise ratio (CNR) between the LV blood and myocardium was also evaluated. These apparent SNR measurements are a suitable method for comparing two acquisition strategies that have largely the same acquisition parameters even when parallel imaging is being used provided the acquisitions otherwise use identical imaging parameters. Statistical differences between SNR and CNR for the two techniques were evaluated using paired, Student t-test with $P < 0.05$. The t-test values were Holm-Sidak posthoc corrected.

RESULTS

Supporting Figure S1, which is available online, shows the Bloch simulation results for the maximum relative FWHM chosen between blood and myocardium tissue signals, the relative deposited RF energy as a surrogate for relative SAR, and the blood–myocardium contrast. The optimal VFA scheme with contrast ≥ CFA = 40°, with relative deposited RF energy < 1 and FWHM of PSF ≤1.2 (relative to CFA) was $\alpha_{high} = 50°$, $\alpha_{low} = 25°$, $N_{low} = 25$, $N_{ramp} = 20$, and $N_{high} = 3$. This VFA scheme resulted in 35% lower SAR than CFA = 40° with relative FWHM = 1.18 and blood–myocardium contrast of 0.11 identical to CFA = 40°. Note that for this VFA scheme, the individual simulated blood and myocardium signals were higher at 0.18 and 0.07, compared with 0.15 and 0.04, respectively for CFA = 40°.

Figure 2 shows example mid-ventricular, short-axis, cardiac cine images acquired in a healthy subject during systolic and diastolic cardiac phases using BH-CFA and the corresponding acquired and reconstructed FB-VFA. When using the optimal FB-VFA scheme the SAR is decreased by 25% compared with BH-CFA. A line profile of the cardiac cine images shows that the blood–myocardium borders are clearly visible in each cardiac phase of the FB-VFA images and are comparable to the BH-CFA acquisition. In an online supplement (Supporting Movie S1), the cardiac cine movies of the acquired real time, multislice, free-breathing data are shown in comparison to the corresponding reconstructed FB-VFA and BH-CFA acquisition.

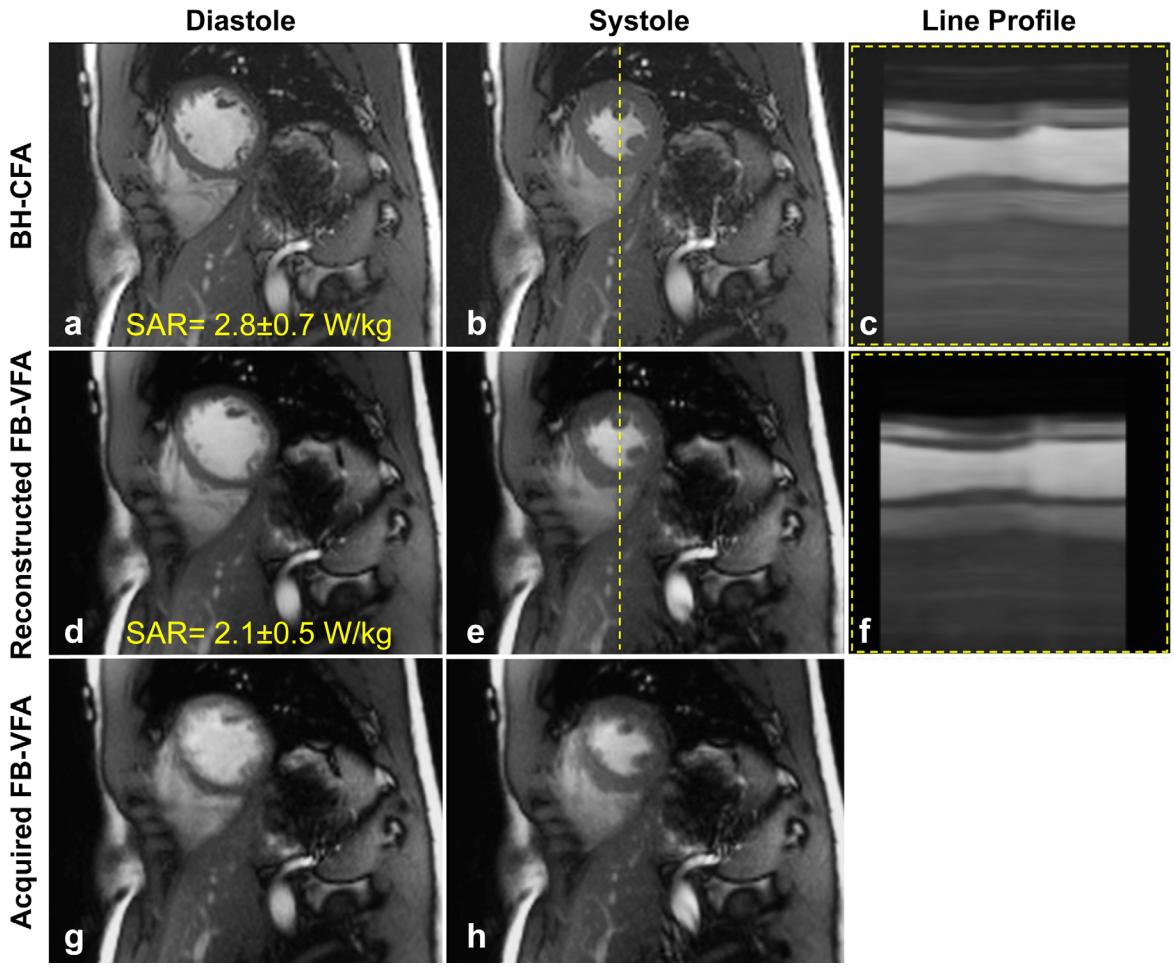

FIG. 2. Diastolic and systolic mid-ventricular short-axis images acquired with breath-hold, constant flip angle (BH-CFA) acquisition (**a,b**), reconstructed free-breathing, bellows-gated, variable flip angle (FB-VFA) acquisition (**d,e**) and the corresponding acquired real-time images (**g,h**). The line profile [dashed line in (b) and (e)] through the cardiac cine images are shown in (**c**) and (**f**) and demonstrate similar blood–myocardium contrast and conspicuity for fine structures.

An example long-axis real-time FB-VFA cardiac images along with the corresponding reconstructed FB-VFA and BH-CFA are shown in Supporting Figure S2 and Supporting Movie S2. These images and movies demonstrate excellent respiratory motion compensation and depiction of cardiac structure and function.

The image quality score for both short-axis and long-axis view images is shown in Table 1. The average score for the short-axis FB-VFA acquisition was significantly lower than the BH-CFA acquisition (3.1 ± 0.5 versus 4.3 ± 0.8, $P < 0.05$). The average score for the long-axis FB-VFA acquisition was also significantly lower than the BH-CFA acquisition (3.4 ± 0.4 versus 4.6 ± 0.6, $P < 0.05$). The image quality of FB-VFA was sufficient to evaluate global and regional cardiac function in both short-axis and long-axis acquisitions. The scores reported by both experts were within 0.5 point of each other for 82.5% of the cases and there were no significant differences between experts ($P > 0.05$).

Table 2 shows the mean LVEF, LVEDV, LVESV, LVSV, and LVEDM for FB-VFA and BH-CFA obtained from 10 healthy subjects. The LVEDV and the LVSV were statistically different between BH-CFA and FB-VFA, with FB-VFA reporting an average of 5% increase in LVEDV and a 12% increase in LVSV. Bland-Altman analysis showed a bias [95%-CI] of 2.5 mL [-9.4, 14.4] for a wide range of LVEDV and LVESV. The linear fit of LVEDV, LVESV, and LVSV between BH-CFA (V_{CFA}) and FB-VFA (V_{VFA}) was $V_{VFA} = 1.02 \bullet V_{CFA} + 2.51$, which indicates BH-CFA estimates of volumes are lower than FB-VFA estimates. The correlation coefficient (R) between the BH-CFA and FB-VFA volumes was 0.98.

Supporting Table S1 shows the measured SNR of the LV blood, RV blood and myocardium and the blood–myocardium CNR for both BH-CFA and FB-VFA at end diastole and end systole. The measured SNR was higher

Table 1
Average Image Quality Score in Mid-ventricular Short-Axis and Long-Axis Images

	Short-axis		Long-axis	
	BH-CFA	FB-VFA	BH-CFA	FB-VFA
Observer-1	4.1 ± 1.0	3.2 ± 0.5	4.7 ± 0.6	3.4 ± 0.5
Observer-2	4.5 ± 0.6	3.0 ± 0.3	4.6 ± 0.6	3.4 ± 0.4

Table 2
Left Ventricular Quantitative Measurements from BH-CFA and FB-VFA Acquisitions.

	BH-CFA	FB-VFA
Ejection fraction (%)	60 ± 6	63 ± 4
End diastolic volume (ml)	128 ± 23	134 ± 21*
End systolic volume (ml)	51 ± 9	49 ± 7
Stroke volume (ml)	77 ± 19	86 ± 17*
End diastolic myocardial mass (g)	95 ± 23	93 ± 23

The asterisks indicate significant differences ($P < 0.05$).

in FB-VFA compared with BH-CFA for all regions. However, only myocardial SNR was significantly different and higher for FB-VFA compared with BH-CFA. The LV blood–myocardium CNR was not significantly different between the two techniques.

Figure 3 shows the end diastolic and end systolic cardiac cine images for a patient with DMD acquired using both FB-VFA and BH-CFA. This patient had a very limited breath-hold capacity and could not hold his breath during repeated BH-CFA acquisitions as evidenced by the motion artifacts (yellow arrows) that are not present in the FB-VFA acquisition.

DISCUSSION

FB-VFA bSSFP can be used for cardiac cine imaging with sufficient image quality for measuring global and regional cardiac function without the need for breath-holding. Herein, Bloch equation simulations were used to determine the VFA scheme that produces blood–myocardium contrast similar to CFA of 40°, with a relative increase in FWHM of PSF $\leq$ 1.2, while reducing the relative RF energy deposition. The maximum limit on the relative increase in FWHM was chosen to be <1.2, based on the previous phantom and in vivo results at 1.5T (9) for different VFA schemes. The maximum myocardial signal in CFA occurs when the FA is in the range of 30° to 40° at 3T (8). In general, the VFA scheme increases the SNR of the stationary myocardium (10) compared with a CFA with the same α_{high}. The flowing blood signal, however, is approximately the same for the VFA and CFA schemes and is largely governed by α_{high} (9). Hence, to maintain the blood–myocardium contrast, the flowing blood signal was increased by using $\alpha_{high} = 50°$ for the VFA scheme at the cost of increasing the relative FWHM of PSF by 1.18. Alternately, α_{high} could have been kept at 40° for the VFA scheme in which case the blood–myocardium CNR would decrease.

The scanner reported SAR is calculated for different time intervals (i.e., 10 s, 90 s, and 360 s). As the BH-CFA sequence was less than 10 s in acquisition duration adding a delay after the scan, during which no scanning can occur, can reduce the average 10 s SAR of this sequence. However, this SAR reduction strategy is not feasible for FB-VFA with acquisition duration of 1 min. This accounts, in part, for

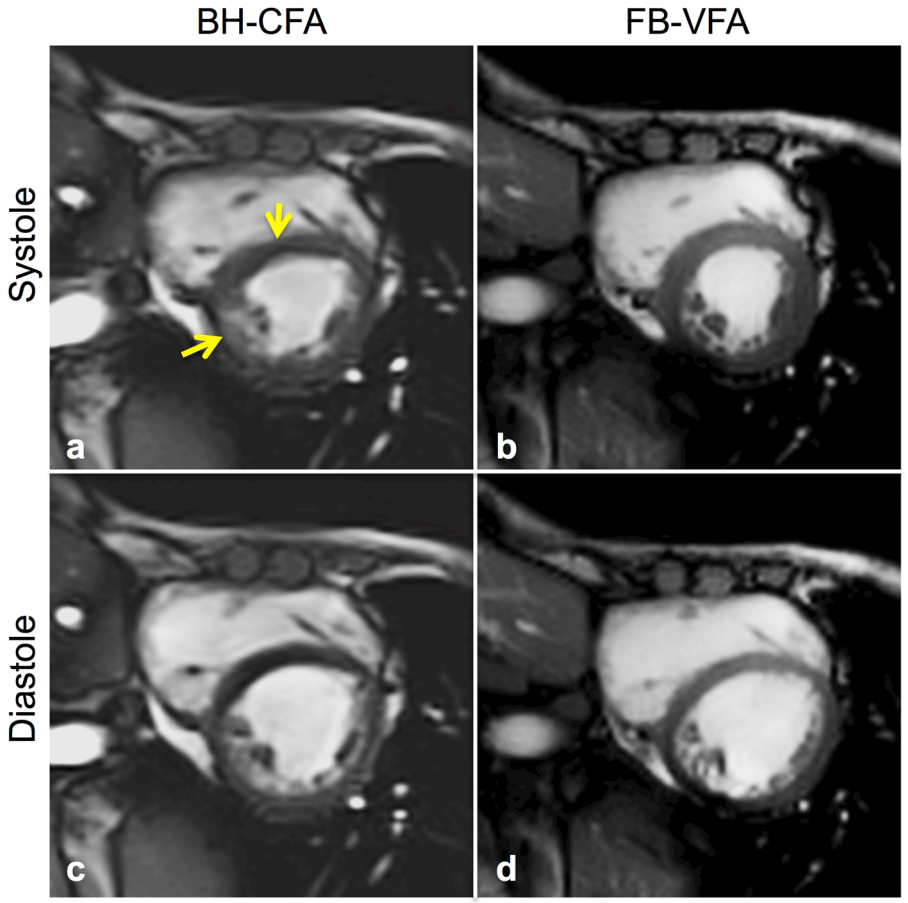

FIG. 3. Systolic (**a,b**) and diastolic (**c,d**) cardiac images from a patient with DMD acquired during instructions for breath-holding with constant flip angle (BH-CFA) acquisition (a,c) compared with free-breathing, variable flip angle (FB-VFA) cardiac cine images (b,d). The myocardial septum has notable image artifacts related to the patient's poor breath-hold abilities (yellow arrows) that are not observable in the FB-VFA images.

the discrepancy between the achievable 25% SAR reduction in in vivo experiments compared with the estimated 35% reduction from Bloch simulations and also due to proprietary SAR calculation methods used by the manufacturer.

Motion compensation using image-based navigators (4,17), to prospectively determine scan specific acquisition duration may be computationally expensive. Alternatively, the respiratory bellows can be used to monitor k-space filling and to prospectively determine the acquisition duration. This can be combined with image-based navigators to retrospectively warp the images within the respiratory window for reduced respiratory motion artifacts. The acquisition duration can also be further reduced using compressed sensing (19).

The image quality score of BH-CFA was higher compared with FB-VFA acquisitions in normal healthy subjects with excellent breath-holding capacity. The acceptable image quality score of FB-VFA demonstrates the potential clinical utility in subjects with poor respiratory function. Lastly, it is important to note that the observed increase in LVEDV and increase in LVSV for FB-VFA compared with BH-CFA accords with the expected differences in LV volumes obtained during free-breathing and breath held exams. Breath-holding is known to transiently increase intrathoracic pressure, which reduces preload and consequently LVEDV. The lower LVEDV leads to a lower stroke volume in accordance with the Frank-Starling effect. Hence, these differences likely reflect normal physiology.

LIMITATIONS

The center frequency of the RF pulse for FB-VFA acquisitions was set based on the BH-CFA acquisitions at the same imaging location. Hence the individual real-time FB-VFA images exhibited more flow-related off-resonance artifacts compared with BH-CFA likely as a consequence of respiratory motion induced shifts in the field and resultant shifts of the off-resonance bands. However, the reconstructed FB-VFA cardiac cine images did not have increased flow-related artifacts compared with BH-CFA (19).

The optimal VFA scheme was optimized for a fixed $N_{ky} = 93$. Further simulations are required to optimize the VFA scheme for changes in N_{ky} as well as changes in the desired blood–myocardium contrast.

The FB-VFA images were acquired for a fixed duration of one minute and retrospectively reconstructed after thresholding of the bellows signal. The retrospective selection of the bellows gating threshold could be automatically set during a scout exam that compares the diaphragm navigator and the bellows signal. This exam could also be used to correct for the phase lag between the diaphragm and the abdominal bellows signal, but requires further investigation. The required acquisition duration can be reduced, by prospectively monitoring the bellows signal.

The clinical evaluation of FB-VFA technique in DMD patients with poor respiratory function is an ongoing study at our Institution and further clinical studies are needed to evaluate its robustness in these and similar patients.

CONCLUSIONS

FB-VFA bSSFP cardiac cine imaging can be used to decrease the SAR of a cardiac cine imaging exam at 3T with image quality sufficient to perform global and regional evaluation of cardiac function.

ACKNOWLEDGMENTS

This work was supported, in part, by funding from UCLA's Center for Duchenne Muscular Dystrophy, the American Heart Association, and Siemens Medical Solutions to D.B.E. The authors thank Francine Cobla for performing quantitative measurements.

REFERENCES

1. Mosqueira M, Zeiger U, Förderer M, Brinkmeier H, Fink RHA. Cardiac and respiratory dysfunction in Duchenne muscular dystrophy and the role of second messengers. Med Res Rev 2013;33:1174–1213.
2. Fayssoil A, Nardi O, Orlikowski D, Annane D. Cardiomyopathy in Duchenne muscular dystrophy: pathogenesis and therapeutics. Heart Fail Rev 2010;15:103–107.
3. Peters DC, Nezafat R, Eggers H, Stehning C, Manning WJ. 2D free-breathing dual navigator-gated cardiac function validated against the 2D breath-hold acquisition. J Magn Reson Imaging 2008;28:773–777.
4. Kellman P, Chefd'hotel C, Lorenz CH, Mancini C, Arai AE, McVeigh ER. High spatial and temporal resolution cardiac cine MRI from retrospective reconstruction of data acquired in real time using motion correction and resorting. Mag Reson Med 2009;62:1557–1564.
5. Nguyen K-L, Khan S, Moriarty J, Mohajer K, Renella P, Satou G, Ayad I, Patel S, Boechat I, Finn JP. CMR in pediatric patients with congenital heart disease: comparison at 1.5T and at 3.0T. J Cardiovasc Magn Reson 2012;14(Suppl. 1):P119.
6. Finn JP, Nael K, Deshpande V, Ratib O, Laub G. Cardiac MR imaging: state of the technology. Radiology 2006;241:338–354.
7. Markl M, Pelc NJ. On flow effects in balanced steady-state free precession imaging: pictorial description, parameter dependence, and clinical implications. J Magn Reson Imaging 2004;20:697–705.
8. Srinivasan S, Ennis DB. Optimal flip angle for high contrast balanced SSFP cardiac cine imaging. Magn Reson Med 2014;73:1095–1103.
9. Srinivasan S, Ennis DB. Variable flip angle balanced steady-state free precession for lower SAR or higher contrast cardiac cine imaging. Magn Reson Med 2014;71:1035–1043.
10. Paul D, Zaitsev M. Improved SNR in linear reordered 2D bSSFP imaging using variable flip angles. Magn Reson Imaging 2009;27:933–941.
11. Ehman RL, McNamara MT, Pallack M, Hricak H, Higgins CB. Magnetic resonance imaging with respiratory gating: techniques and advantages. AJR Am J Roentgenol 1984;143:1175–1182.
12. Santelli C, Nezafat R, Goddu B, Manning WJ, Smink J, Kozerke S, Peters DC. Respiratory bellows revisited for motion compensation: preliminary experience for cardiovascular MR. Magn Reson Med 2011;65:1097–1102.
13. Markl M, Alley MT, Elkins CJ, Pelc NJ. Flow effects in balanced steady state free precession imaging. Magn Reson Med 2003;50:892–903.
14. Stanisz GJ, Odrobina EE, Pun J, Escaravage M, Graham SJ, Bronskill MJ, Henkelman RM. T1, T2 relaxation and magnetization transfer in tissue at 3T. Magn Reson Med 2005;54:507–512.
15. Griswold MA, Jakob PM, Heidemann RM, Nittka M, Jellus V, Wang J, Kiefer B, Haase A. Generalized autocalibrating partially parallel acquisitions (GRAPPA). Magn Reson Med 2002;47:1202–1210.
16. Deshpande VS, Shea SM, Li D. Artifact reduction in true-FISP imaging of the coronary arteries by adjusting imaging frequency. Magn Reson Med 2003;49:803–809.
17. Hansen MS, Sørensen TS, Arai AE, Kellman P. Retrospective reconstruction of high temporal resolution cine images from real-time MRI using iterative motion correction. Magn Reson Med 2012;68:741–750.
18. Dietrich O, Raya JG, Reeder SB, Reiser MF, Schoenberg SO. Measurement of signal-to-noise ratios in MR images: influence of multichannel coils, parallel imaging, and reconstruction filters. J Magn Reson Imaging 2007;26:375–385.

19. Xue H, Kellman P, Larocca G, Arai AE, Hansen MS. High spatial and temporal resolution retrospective cine cardiovascular magnetic resonance from shortened free-breathing real-time acquisitions. J Cardiovasc Magn Reson 2013;15:102.

SUPPORTING INFORMATION

Additional Supporting Information may be found in the online version of this article.

SUP. FIG. S1. Bloch simulation of the relative full width half maximum (FWHM) of the point spread function (**a–c**), relative sum of squares of the variable flip angle (VFA) scheme (**d–f**) with respect to constant flip angle of 40°, and contrast between flowing blood and stationary myocardium signal (**g–i**) for varying number of ramp pulses (N_{ramp}) and number of low pulses (N_{low}) for $\alpha_{low} = 10°$ (a,d,g), $\alpha_{low} = 25°$ (b,e,h), and $\alpha_{low} = 40°$ (c,f,i) with constant $\alpha_{high} = 50°$ and $N_{ky} = 93$. The blood–myocardium simulation with constant flip angle (CFA) of 40° resulted in a relative FWHM of 1, relative sum of squares of the flip angles = 1, and contrast = 0.11 as indicated in the color bars. The VFA scheme which produced the least relative sum of squares of the flip angle (0.65) with contrast similar to CFA of 40°, and with relative FWHM = 1.18 is $N_{low} = 25$, $N_{ramp} = 20$, $\alpha_{low} = 25°$, and $\alpha_{high} = 50°$ are shown in the black circles. **j:** The corresponding optimal VFA blood (magenta) and myocardium (blue) steady-state signals are shown as solid lines and are compared with CFA = 40° (dashed lines).

SUP. FIG. S2. Four chamber diastolic and systolic real-time cardiac images acquired during free-breathing with variable flip angles (FB-VFA) (**a,d**) and the corresponding reconstructed FB-VFA cardiac cine images (**b,e**) show a clearer depiction of the valves (arrows) and improved myocardial wall sharpness comparable to the breath-hold constant flip angle (BH-CFA) acquisition (**c,f**).

Supporting Table S1. Signal to noise ratio (SNR) and contrast to noise ratio (CNR) measured in mid-ventricular short-axis slice in 10 healthy subjects. The asterisk indicates significant differences ($P < 0.05$).

Supporting Movie S1. The acquired short-axis free-breathing, real time cardiac images with a temporal footprint of 263 ms (top row) was reconstructed into the FB-VFA cardiac cine images (middle row). The corresponding BH-CFA cardiac cine images acquired at the same slice locations are shown in the bottom row. Detailed cardiac wall motion (including atrial kick) and fine papillary and trabecular muscle structure are seen with good respiratory motion compensation in the FB-VFA images and compare favorably with the conventional BH-CFA acquisitions.

Supporting Movie S2. Example four-chamber free-breathing, real time cardiac images acquired from a healthy subject (left) with the corresponding reconstructed cardiac cine images of FB-VFA (middle) and conventional BH-CFA (right). The excellent respiratory motion compensation in FB-VFA is apparent in the chest wall. The myocardial wall and the papillary muscles are also clearly depicted in FB-VFA indicating good respiratory and cardiac motion compensation.